Biophysical Chemistry 143 (2009) 145–153

Contents lists available at ScienceDirect

Biophysical Chemistry

journal homepage: http://www.elsevier.com/locate/biophyschem

# Self assembly of poly(o-methoxy aniline) with RNA and RNA/DNA hybrids: Physical properties and conformational change of poly(o-methoxy aniline)

Parimal Routh, Pratap Mukherjee, Arnab Dawn, Arun K. Nandi *

*Polymer Science Unit, Indian Association for the Cultivation of Science, Jadavpur, Kolkata-700 032, India*

ARTICLE INFO

*Article history:*
Received 26 March 2009
Received in revised form 8 May 2009
Accepted 13 May 2009
Available online 22 May 2009

*Keywords:*
Self assembly
RNA
DNA
Poly(o-methoxy aniline)
Conformational change
Conductivity

ABSTRACT

Biomolecular hybrids of a conducting polymer [poly(*o*-methoxy aniline) (POMA)] and RNA are prepared at the three different compositions by mixing aqueous solutions of diethyl, 2-hydroxy ethyl, ammonium salt of RNA (type IX from Torula Yeast) and POMA (ES, emeraldine salt; doping level [Cl]/[N] = 0.52). A slow increase of pH up to 30 h of aging occurs in the mixture till it levels up. The TEM micrographs indicate a fibrillar network structure in all the hybrid compositions (POMA: RNA = 1:3, 1:1, 3:1, by weight). In the complexes three types of supramolecular interactions, viz. (i) electrostatic, (ii) H-bonding and (iii) $\pi$–$\pi$ interactions, are evident from the FTIR spectroscopy. The CD spectra indicate a small distortion of A-RNA conformation towards its B form during the hybrid formation. Time and temperature dependent UV–vis spectral studies indicate a slow red shift of the $\pi$-band to polaron band transition peak ($\lambda_{max}$) for the uncoiling of the POMA (P) chain on the RNA (R) surface. The repulsive interaction between the radical cations of POMA (ES) absorbed on the RNA surface is attributed to the conformational change causing the uncoiling of POMA chain. UV–vis spectral study indicates that the uncoiling and attachment of POMA on RNA surface is much faster than that on DNA (D). In POMA–RNA–DNA (PRD) hybrid solutions slower red shift of $\lambda_{max}$ indicates more disordered array of the phosphate groups than that in PR and PD systems. The conductivity values of the PR hybrids ($10^{-6}$ S/cm$^{-1}$) are three orders higher than that of RNA, rendering the PR hybrids to be useful for fabricating good biosensors. In the PRD hybrids conductivity decreases by two orders than those of PR and PD hybrids suggesting a disorder arrangement of POMA chains in the PRD hybrids. The *I–V* characteristic curves of the PR and PRD hybrids indicate a semiconducting nature of the hybrids.



## 1. Introduction

The immobilization of conducting polymers on the DNA surface is a fascinating area of research for its application in DNA diagnostics [1–3], DNA-hybridization [4,5], gene therapy [1,6], genoelectonic [1,6] and in various biosensing applications [2,3,7–10]. Like DNA, ribonucleic acid (RNA) is an important biological macromolecule that plays several important roles in the biological activity of living cells [11,12]. It is a carrier of genetic information from DNA to proteins, a messenger between DNA and protein synthesis complexes and acts as a carrier molecule of amino acids for protein synthesis. So it is necessary to monitor the state of an RNA molecule to understand the cell processes more explicitly and one possible way is to immobilize a conducting polymer on the RNA surface, because the electro-active nature of the conducting polymer may detect the state of RNA molecules. There are few reports where different types of supramolecular interactions are exploited to make the hybrids of RNA and polyaniline (PANI) [13,14]. In the poly(aniline boronic acid) (PABA)–RNA multilayer hybrid, PABA interacts covalently with RNA through formation of (i) boronate esters, (ii) boron nitrogen dative bond and (iii) electrostatic interaction. The multilayer hybrid provides controlled release of RNA through redox process, making it useful in biomedical and therapeutic applications [13]. Recently, Gao et al. utilized the electrostatic interaction of micro (mi) RNA and cationic PANI to make hybrid of PANI nanowires with mi-RNA [14]. This material acts as a good biosensor for detection of mi-RNA in the total RNA coming from the cancer cells. Besides in the conducting polymer–RNA hybrids, gold nanoparticle tagged RNA materials are also used for structural characterization of protein–RNA complexes [15]. The shape of Pd nanoparticles in the RNA mediated synthesis of palladium nanoparticles on gold surfaces is dictated by the RNA sequence [16]. Thus there are some reports of RNA-conducting polymer hybrids and to understand the structure, morphology, spectral properties, conductivity etc. in general, more study on the hybrids of RNA with different conducting polymers is necessary. We report here the immobilization of RNA with a conducting polymer, poly(*o*-methoxy aniline) (POMA). Due to the presence of the ortho methoxy group, POMA is soluble in water [17,18] and its emeraldine salt has numerous number of radical cation centers (Scheme 1). The electrostatic attraction between the radical cations of POMA and the RNA anions would be a suitable force for the immobilization of POMA on the RNA surface. Here we have exploited this technique to produce the RNA–POMA biomolecular hybrid.

* Corresponding author.
*E-mail address:* psuakn@mahendra.iacs.res.in (A.K. Nandi).

0301-4622/$ – see front matter © 2009 Elsevier B.V. All rights reserved.
doi:10.1016/j.bpc.2009.05.004

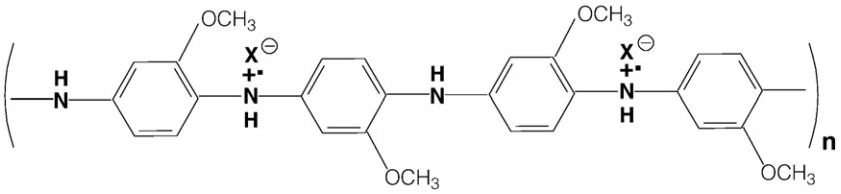

**Scheme 1.** Poly(*o*-methoxy aniline) (emeraldine salt, ES) $X^-$=$Cl^-$ ion.

Recently, we have reported the hybrid formation of double stranded (ds) DNA and POMA by using (i) the acid form of DNA and POMA (emeraldine base, EB) through acid–base interaction [17] and (ii) the salt from of DNA and POMA (emeraldine salt, ES) through ionic interaction [18]. In both cases a continuous red shift of the $\pi$-band to polaron band transition peak is observed in the UV–vis spectra of hybrid solutions with aging time (up to 2 days). The slow red shift has been explained from the slow uncoiling of POMA chain on the DNA surface. DNA has a very large surface area where the adsorbed POMA molecules can experience a stable electrostatic repulsion between the radical cations of POMA causing the uncoiling of POMA chains. RNA has also a very large surface area and so a similar red shift of the $\pi$ to polaron band transition peak due to the uncoiling of POMA chains is expected in the PR system. Due to the difference in the structures of DNA and RNA, some differences in the uncoiling and complexation rates with the conducting polymer are expected and would be worked out here.

During transcription of the protein-coding genes, RNA forms a stable elongation complex with DNA [19,20]. So the addition of POMA on this DNA–RNA hybrid (PDR system) may behave differently, particularly in the variation of $\pi$-band to polaron band transition peak with time. In this article we also present the changes of UV–vis spectra of POMA with time in these PDR hybrids. Here we have compared the rate of uncoiling of POMA chains in the duplexes of POMA–RNA with POMA–dsDNA and also with that of triplexes of POMA–dsDNA–RNA system. Besides, both DNA and POMA are nonconducting ($s \leq 10^{-12}$ S/cm) but the hybrids are semiconducting ($s = 10^{-7}$ S/cm) [17,18]. So we also expect a good conductivity in the RNA–POMA system, which may find its use in developing biosensors to be useful for characterizing the state of RNA in a biological process. The conductivity of the PRD triplexes, may differ from that of PD or PR duplexes and would also be reported here with the possible reasons.

## 2. Experimental

### 2.1. Sample

The RNA sample, a product of Sigma Chemicals, USA is a diethyl amino ethanol salt from Torula Yeast (type IX, product no. R3629-5g). Calf thymus DNA (type 1; sodium salt) is also purchased from Sigma Chemicals, USA. POMA is synthesized in the laboratory in 1.0 M HCl containing 5.8 M LiCl at a low temperature [21]. Molar ratios of the reactants are 1.0:4.3:39.6 for ammonium peroxydisulfate, *o*-methoxy aniline, and 1.0 M HCl, respectively. They are mixed at −35 °C and the reaction mixture is kept for 2 days at −18 °C. The polymer produced is separated by filtration and washed repeatedly with water. It is stirred with 0.1 M $NH_4OH$ solution for 2 days and is then dried in vacuum to get the emeraldine base (EB) from of POMA. The molecular weight of the sample is determined from the intrinsic viscosity measurement in 97% $H_2SO_4$ at 25 °C and have a value of $\bar{M}_v = 20{,}900$ (taking Mark–Houwink constant $K = 1.95 \times 10^{-6}$ and $\alpha = 1.36$) [17,22,23].

### 2.2. Hybrid preparation

The RNA and DNA solutions (0.02% w/v) are produced by mixing required amount of RNA and DNA in the triple distilled water (pH 6.9) and by keeping them for 24 h at 30 °C. The RNA solution has a pH equal to 7.8. The emeraldine salt of POMA (ES) is prepared by mixing 6 ml 0.001 N HCl solution with 30 ml 0.005% (w/v) POMA (EB) solution for 30 min. The doping level is measured from the elemental analysis and is found to be [Cl]/[N] = 0.52. The resulting POMA (ES) solution (0.0042% w/v) is transparent and greenish blue. The blends of different compositions (w/w) are prepared by mixing the above RNA solution with the POMA (ES) solution in different proportions and leaving them for 7 days at room temperature (30 °C). The solutions are then freeze-dried to study the structure and conductivity of the hybrids. For this purpose the sample solutions are taken in a 100 ml round bottomed flask and are then frozen by dipping into liquid nitrogen. These frozen materials are inserted in the limbs of the Vir Tis freeze-drier (Model 2KBTES-55) and dried by applying vacuum at 40 mTorr. The freeze-dried samples are further dried in a vacuum desiccator for 7 days to get rid of the solvent, completely. The pH of the hybrid solutions are monitored with aging time using a pH meter (Denver Instrument, model 50). The hybrid samples are designated as PR31, PR11 and PR13, where POMA (P) and RNA (R) are present in the respective weight ratios indicated by the numbers.

The hybrids of POMA, RNA and DNA are prepared by mixing 0.02% (w/v) Na–DNA solution (in tripled distilled water) to the above solutions of POMA (ES) and RNA in different proportions to make the PRD hybrids designated as PRD133, PRD111 and PRD311 where the numbers indicate weight ratios of the respective components.

### 2.3. Morphology

The TEM micrographs of the samples are made by dropping a drop of 7 day aged hybrid solutions on the carbon coated copper grids and drying at 30 °C in air and finally in vacuum. The micrographs are taken from a high resolution transmission electron microscope (JEOL, 2010EX) operated at an accelerated voltage of 200 kV fitted with a CCD Camera.

### 2.4. Spectroscopy

The CD spectra of aqueous RNA solution, POMA solution and POMA–RNA hybrid solutions are made in a spectro polarimeter (JASCO, model J-815) in a 1 cm quartz cuvette at 30 °C after 4 days of aging. The UV–vis spectra for the different aging times are taken from aqueous solutions of the hybrids in 1 cm quartz cell from 190 to 1100 nm using a UV–vis spectrophotometer (H.P, model 8453). The FTIR spectra of the freeze-dried samples are made from a Nicolet FTIR instrument (Magna IR-750 spectrometer (series 11)). The sample is mixed with solid KBr and pellets are made to scan the sample. Subtraction of the POMA spectra from the RNA–POMA spectra is made using the Omnic software attached to the instrument to understand the interaction of RNA with POMA.

### 2.5. Conductivity measurement

The dc conductivity of the freeze-dried samples is measured by the two-probe method. The conductivity is measured by taking the

sample between two indium–titanium oxide (ITO) conducting strips of 1 mm width placed perpendicularly. The detailed procedure is presented in our earlier publication [24]. All the measurements are carried out in vacuum. The area of the sample is 0.01 $cm^2$ and the thickness of the samples is measured by a screw gauge. The conductivities of the sandwiched samples are measured by an electrometer (Keithley, model 617) at 30 °C using the following equation:

$$\sigma = \frac{1}{R} \times \frac{l}{a}$$

where '$l$' is the thickness, '$a$' is the area and '$R$' is the resistance.

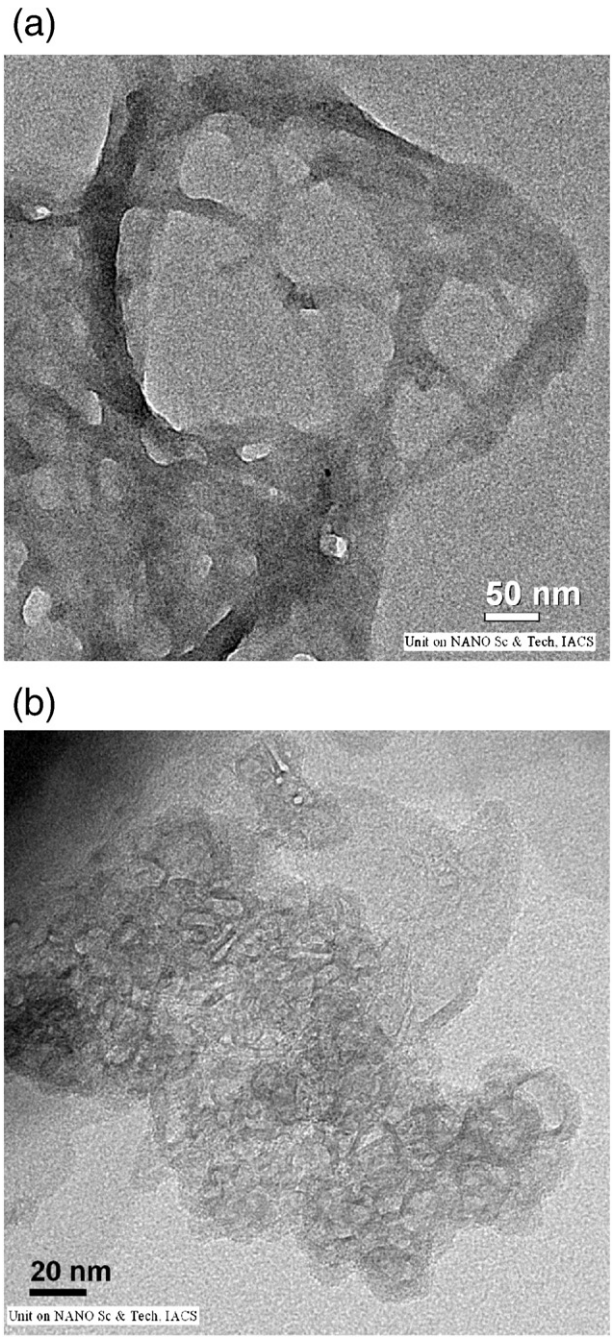


**Fig. 1.** TEM micrographs of (a) PR11 hybrid and (b) pure RNA.

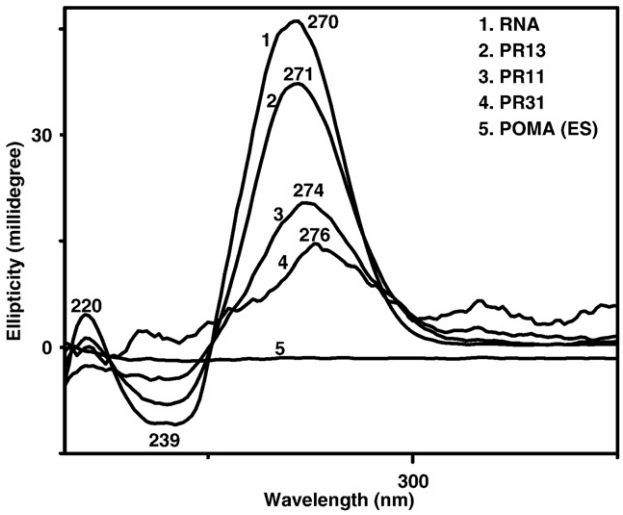


**Fig. 2.** Normalized CD spectra at 30 °C of RNA, POMA (ES) and RNA–POMA hybrid (PR31, PR11 and PR13) solutions with respect to RNA.

The *I–V* characteristic curves of the samples are studied using the same sample by applying voltage from −5 to +5 V and the current is measured at each applied voltage.

## 3. Results and discussion

### 3.1. Morphology

In the TEM micrographs (Fig. 1(a, b)) the morphology of PR11 and pure RNA is presented. PR11 exhibits fibrillar network structure as in the pure RNA. The fibrillar network structure is also observed in PR31 and PR13 hybrids (Suppl. Fig. 1). From the morphological study it may be concluded that like the PD hybrids [17,18] RNA produces bimolecular hybrids with POMA having a fibrillar network structure.

### 3.2. Circular Dichroism (CD)

The normalized CD spectra of the four day aged hybrid solutions are presented in Fig. 2. RNA shows a strong peak at 270 nm and the intensity of 270 nm peak decreases significantly with increasing POMA concentration. There is also a small red shift of the peak

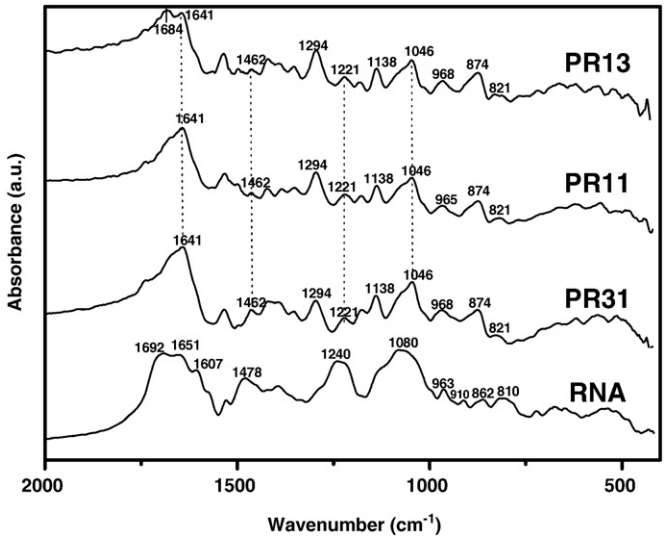


**Fig. 3.** FTIR spectra of pure RNA and POMA subtracted POMA–RNA hybrids (PR31, PR11 and PR13).

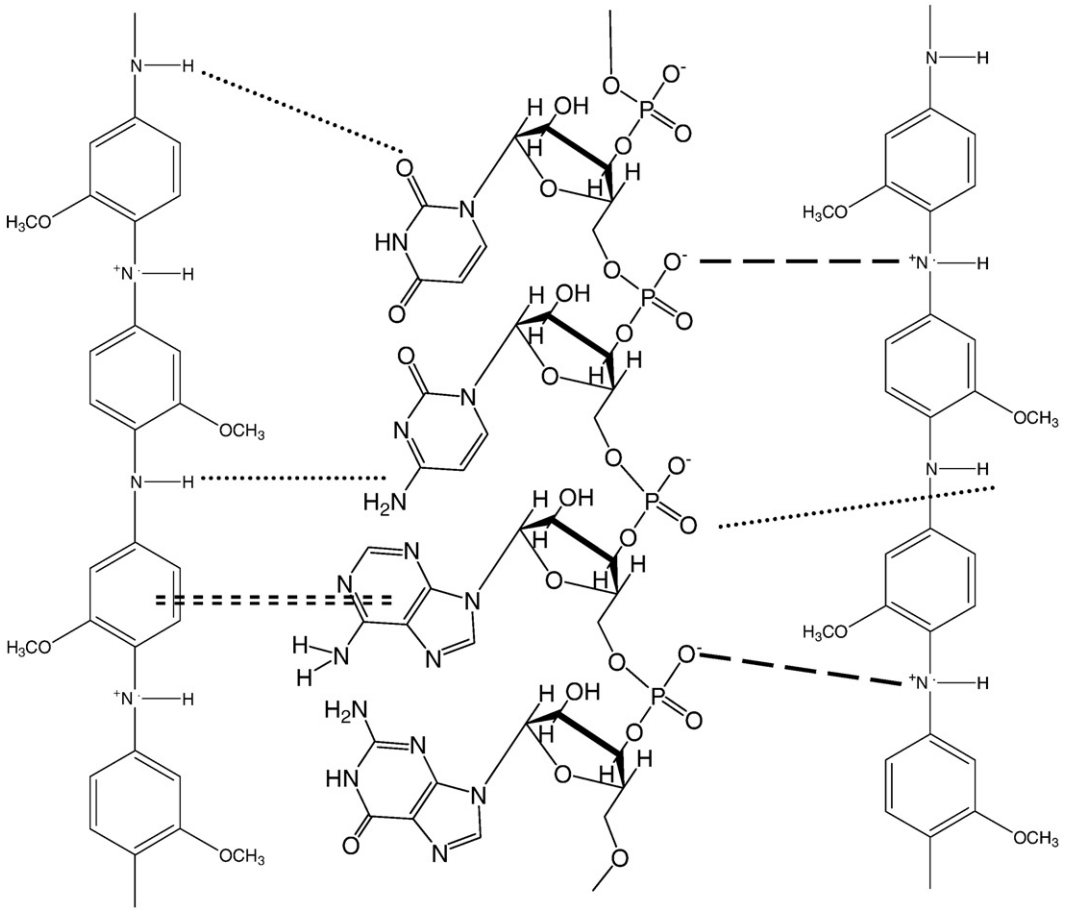

**Scheme 2.** Illustration of RNA–POMA (ES) interaction demonstrating ionic, hydrogen bonding and $\pi$–$\pi$ interactions. [Ionic: _____, Hydrogen bonding: ..... and $\pi$–$\pi$ interaction: = = = = =].

position with increasing the POMA concentration in the hybrid. The chain conformation presented in the CD spectra is for A-RNA. In the hybrids the shapes of CD spectra are very similar to that of pure RNA indicating that the overall conformation of RNA in the hybrids is in the A-form. The decrease of intensity and a small red shift of 270 nm peak in the hybrids indicate a small distortion of 'A' helix towards 'B' form [25,26]. This could imply that the narrow major groove as found in regular A-helix of the pure RNA may be widened on binding with POMA [25a].

### 3.3. FTIR spectra

The nature of molecular interactions between POMA and RNA can be determined from the FTIR spectra presented in Fig. 3 (Suppl. Fig. 2 for POMA). RNA has IR absorption peaks for the in-plane vibrations at 1692 $cm^{-1}$ (G and U), 1651 $cm^{-1}$ (U, G, A, and C); 1607 $cm^{-1}$ (A); 1481 $cm^{-1}$ (C) and 1240 $cm^{-1}$ ($PO_2$ asymmetric stretching) [25b,27–31]. [G = guanine, U = uracil, A = adenine, C = cytosine]. Also there are peaks

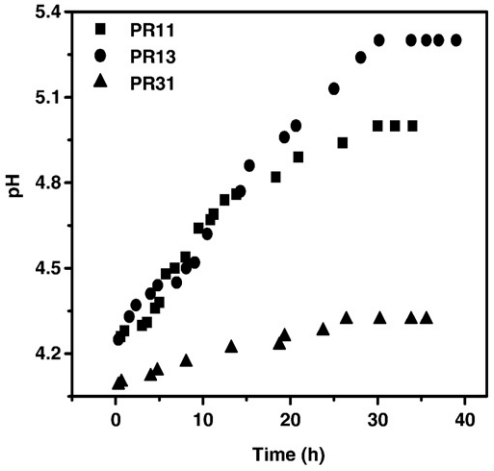


**Fig. 4.** Plot of pH vs. aging time in PR13, PR11 and PR31 hybrid at 30 °C.

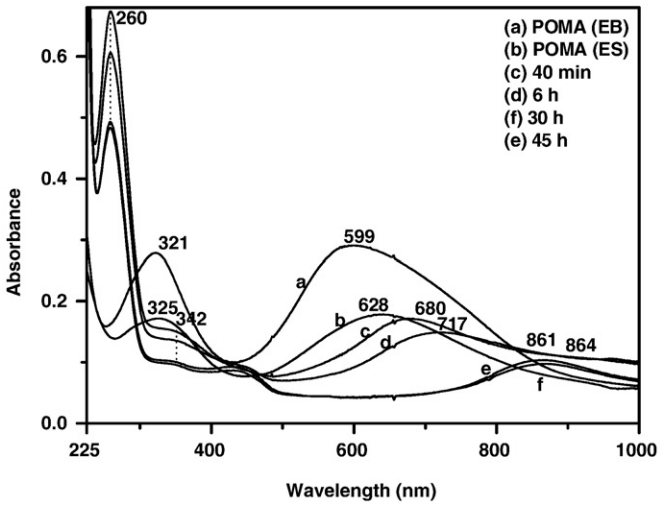


**Fig. 5.** UV–vis spectra of POMA (EB), POMA (ES), and POMA–RNA hybrid (PR11) solutions at indicated aging time at 30 °C.

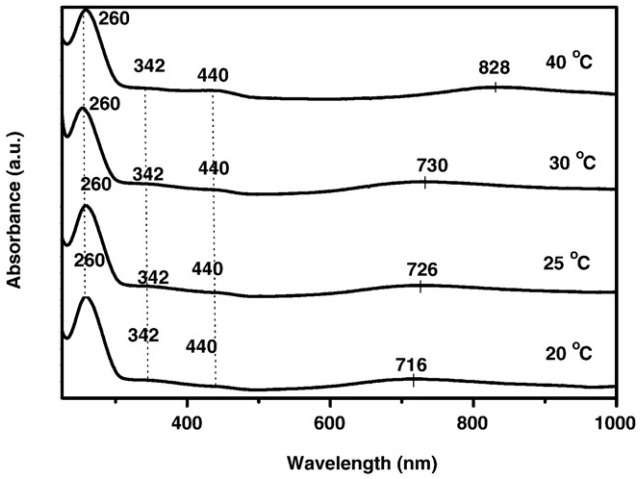


**Fig. 6.** UV–vis spectra of POMA–RNA hybrid (PR11) at indicated temperatures for 8 h of aging.

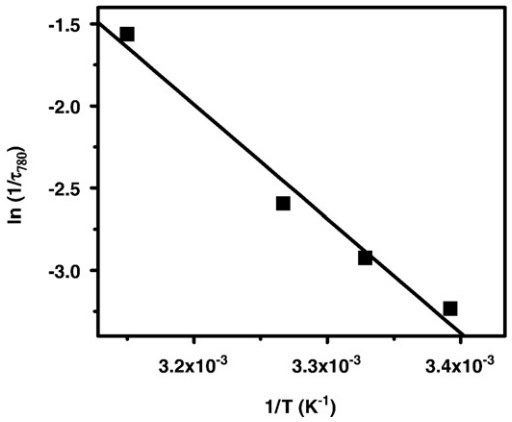


**Fig. 8.** Representative Arrhenius plot of ln $(1/\tau_{780})$ vs. $1/T$ $(K^{-1})$ for PR11 hybrid.

at 810 and 862 $cm^{-1}$ corresponding to the ribose-phosphate vibrations indicating that the RNA used here is A-RNA [32–35]. In the POMA–RNA hybrid the asymmetric stretching frequency of P═O group shifts from 1240 $cm^{-1}$ to 1221 $cm^{-1}$ for all the hybrids. The shift of 1240 $cm^{-1}$ to 1221 $cm^{-1}$ in all the hybrids indicates a small distortion of A-helix towards B-helix as well as for the formation of H bond between the phosphate group of RNA and POMA [25]. Also the symmetric stretching peak at 1080 $cm^{-1}$ of P═O group of RNA is shifted to 1046 $cm^{-1}$ in all the hybrids due to the H-bonding interaction. In the PR13 hybrid, the 1692 $cm^{-1}$ band shifts to 1684 $cm^{-1}$ and the same peak is completely lost in the other two hybrids (PR11 and PR31). One probable reason is the complexation of G and U bases with POMA and the complete complexation at higher POMA concentration inhibits the in-plane vibration of G and U bases. Probably, the –C═O groups of G and U form H bonds with –NH– groups of POMA inhibiting the in-plane vibration. The in-plane vibration frequency of 1651 $cm^{-1}$ of U, G, A, and C shifted to lower wave number 1641 $cm^{-1}$ indicating that the $\pi$ clouds of U, G, A, and C rings are somewhat delocalized through the $\pi$ clouds of POMA rings by $\pi$–$\pi$ interactions decreasing the in-plane vibration frequency. A trace amount of water may partially obscure the U, G, A, and C in-plane vibrations at 1600–1700 $cm^{-1}$ because of the –OH bending vibration of water [30]. However, our samples are perfectly dried as there is no difficulty in assigning the various in-plane vibrations of the bases. The 1607 $cm^{-1}$ peak of adenine is lost in every hybrid, indicating that the in-plane vibration of adenine is totally ceased due to the complexation with RNA through weak H bond interaction of amino group [25(a),31]. This is also supported from the appearance of the above peak as a hump for the PR13 hybrid (1606 $cm^{-1}$) indicating that the hump is caused by the excess RNA. The in-plane vibration of cytosine at 1481 $cm^{-1}$ [25(a)] is shifted to lower frequency at 1462 $cm^{-1}$ for all the hybrids, advocating the $\pi$–$\pi$ interaction of POMA (ES) with cytosine base. The humps at 1137 $cm^{-1}$ and 1294 $cm^{-1}$ of RNA become prominent peaks in the POMA–RNA hybrids, the reasons are unknown. Thus there exists (i) electrostatic interaction between radical cations of POMA (ES) and phosphate anion of RNA, (ii) H-bonding interaction of –NH– group of POMA (ES) with P═O group and U, G, A, and C bases of RNA; and (iii) $\pi$–$\pi$ interaction of phenyl rings of POMA with $\pi$-clouds of RNA bases. All the interactions are schematically shown in Scheme 2. These large numbers of supramolecular interactions make the RNA–POMA hybrid stable.

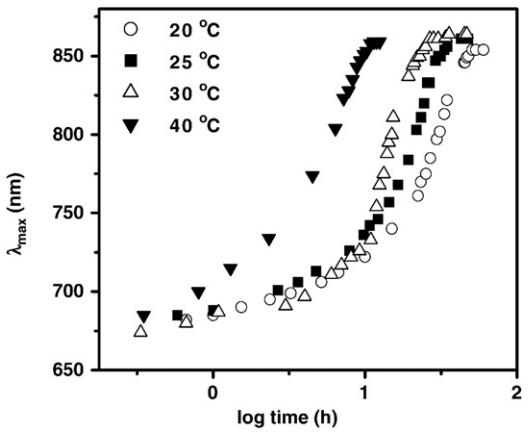


**Fig. 7.** $\lambda_{max}$ of the $\pi$ band to polaron band transition at 20 (○), 25 (■), 30 (△) and 40 °C (▼) plotted against log time for POMA–RNA (PR11) hybrid solution.

### 3.4. pH Study

In Fig. 4 the change of pH with aging time of the hybrid solutions is plotted for the different compositions of the hybrid and it is interesting that there is an initial increase of pH with time up to 30 h of aging and finally there is a leveling of pH, whose value depends on the composition of the hybrid. The PR13 levels up at pH 5.3, PR11 at pH 5.0 and it is 4.2 for PR31. The rate of increase (i.e. initial slope) of pH with time is the same for PR13 and PR11 samples. The probable reason for the slow change in pH with time is due to the slow complexation arising from the different supramolecular interactions. The pH of the POMA (ES) solution is 3.86 and that of RNA solution is 7.8. On mixing the components in different proportions after 30 min of mixing the pH values are 4.1, 4.25 and 4.27 for PR31, PR11 and PR13, respectively. This initial jump of pH is due to the formation of POMA–RNA complex and the increase of pH with time is indicative of complexation. The POMA (ES) is a salt of weak base and strong acid, consequently the pH of the POMA (ES) solution is in acidic range (pH = 3.86) but the RNA with a quaternary ammonium salt is the salt of a weak acid and a weak base, so it should have pH near the neutral value (pH = 7.8). On addition of RNA to POMA solution there are three types of species (i) PR complex, (ii) unbound RNA and (iii) unbound POMA, the concentrations of which dictate the pH of the medium. So, the greater the concentration of RNA in the hybrid, the larger is the

**Table 1**
Activation energy values of uncoiling of POMA in POMA–RNA, POMA–DNA, POMA–RNA–DNA systems.

| Composition of PR hybrid | Activation energy (kcal/mol) | Composition of PD hybrid | Activation energy (kcal/mol) | Composition of PRD hybrid | Activation energy (kcal/mol) |
|---|---|---|---|---|---|
| PR13 | 15.3 | PD13 | 14.9 | PRD133 | 12.3 |
| PR11 | 14.3 | PD11 | 14.5 | PRD111 | 14.0 |
| PR31 | 12.5 | PD31 | 13.1 | PRD311 | 13.1 |

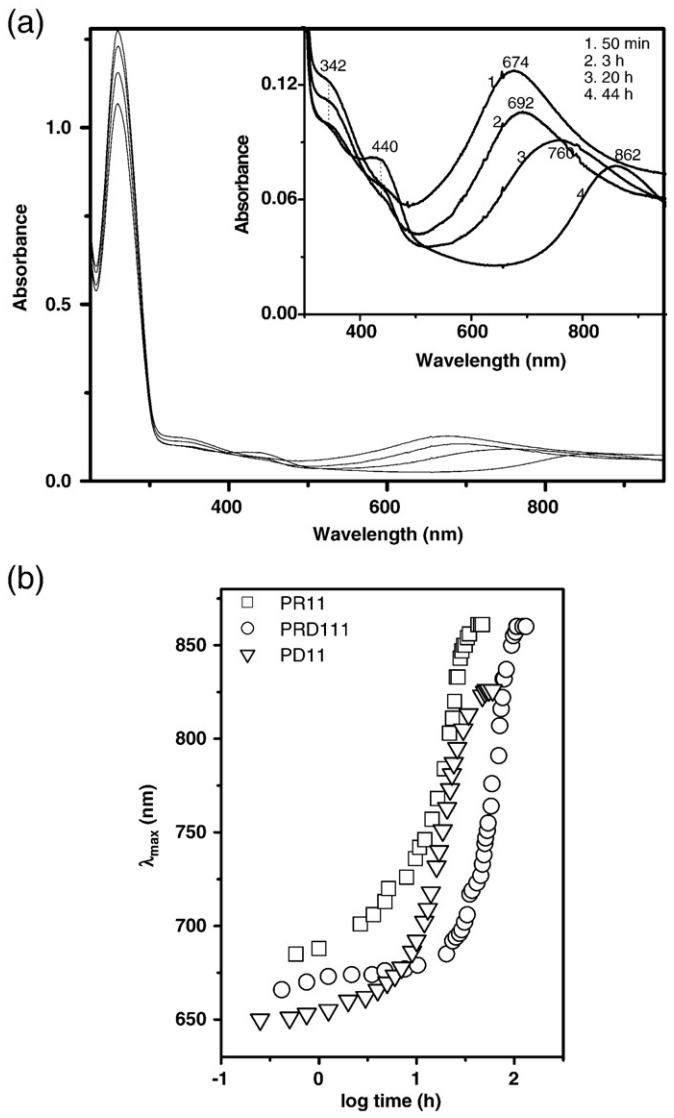


**Fig. 9.** (a). UV–vis spectra of POMA–RNA–DNA hybrid (PRD111) solution at different aging times at 30 °C. (b). Comparison of $\lambda_{max}$ of the $\pi$ band to polaron band transition of PRD111 (○), PR11 (□) and PD11 (▽) plotted against log time (h) for hybrid solutions at 25 °C.

equilibrium concentration of uncomplexed RNA causing the pH of the mixture higher. The PR complex is somewhat different from POMA (ES) in the light of the proton dissociation equilibrium. In POMA (ES) the proton can more easily dissociate than that in the PR complex because of the increased stability of cationic charge by $RNA^-$ through electrostatic binding. This stabilization of cationic charge causes a lesser feasibility of protons to come out of the complex. Consequently, as the complex is produced proton concentration in the medium decreases increasing pH with time. It is evident from the figure that pH increases up to ~30 h i.e. the equilibrium complexation is reached in 30 h of aging, indicating that the PR complexation is a slow process.

### 3.5. UV–vis spectra

In Fig. 5 the UV–vis spectra of PR11 at 30 °C (Suppl. Fig. 3 for PR13 and PR31) is presented to understand the doping behavior with time. The POMA (EB) has a peak at 321 nm for the $\pi$–$\pi^*$ transition of benzonoid ring and a 599 nm peak corresponding to the electronic excitation from benzonoid to quinonoid ring [36–39]. In the POMA (ES) the later peak is lost and a new peak at 628 nm for the $\pi$-band to localized polaron band transition is observed. On addition of POMA (ES) to RNA solution this $\pi$-band to polaron band transition peak shifts to 680 nm which shows a further gradual red shift with aging time and becomes invariant at 864 nm. The $\pi$–$\pi^*$ transition band of the benzonoid ring also shifts from 321 to 342 nm and a new band appears at 440 nm corresponding to the transition of polaron band to $\pi^*$ band.

#### 3.5.1. Shift of π-band to polaron band transition in POMA–RNA (PR) system

The gradual red shift of the polaron band transition with aging time is similar to that of POMA–DNA hybrid [17,18] and the reason may be for the increase of conjugation length of POMA chain due to its uncoiling by the repulsive interaction between radical cations of POMA adsorbed on RNA surface. Due to the physical binding of POMA (ES) on the RNA surface, the conformational transition arising from the repulsion of radical cations of POMA becomes stable. A support of the above assertion may be obtained from the temperature dependent UV–vis study of the hybrid solution. A representative figure for temperature variation of UV–vis study is shown in Fig. 6 for the same time (viz. 8 h) of aging of PR11 sample. It is evident from the figure that the $\pi$-band to polaron band transition peak shifts to higher wavelength with temperature, indicating that the rate of conformational transition increases at higher temperatures. Fig. 7 shows the $\lambda_{max}$ vs. log time plot of the $\pi$-band–polaron band transition peak for PR11 sample (Suppl. Fig. 4 for PR13 and PR31). It is apparent from the figure, that initially there is a slow increase of $\lambda_{max}$ with log time and then there is a rapid increase and finally it levels up, indicating auto catalytic nature of the process. After adsorption of the POMA chain on the RNA surface repulsion between radical cations occurs in a co-operative manner causing a sigmoidal rise of $\lambda_{max}$ with time. It is apparent from the figure that there is a strong temperature dependency and higher the temperature, faster is the uncoiling rate causing faster red shift. The leveling value of $\lambda_{max}$ is almost constant for all the temperatures and in every temperature the autocatalytic nature persists. A comparison with that of the PD system [18(a)] indicates that in the PR system the initial parts of the plots are not as flat as in the former case, indicating that the uncoiling of POMA in the

**Table 2**
Comparison of the rates ($1/\tau_{780}$) of uncoiling of POMA chain in the PD, PR and PRD systems.

| Temperature (°C) | Composition | $1/\tau_{780}\times10^{-2}$ ($h^{-1}$) | Composition | $1/\tau_{780}\times10^{-2}$ ($h^{-1}$) | Composition | $1/\tau_{780}\times10^{-2}$ ($h^{-1}$) |
|---|---|---|---|---|---|---|
| 20 | PD11 | 2.6 | PD13 | 1.7 | PD31 | 2.3 |
| | PR11 | 3.9 | PR13 | 4.0 | PR31 | 3.4 |
| | PRD111 | 1.6 | PRD133 | 0.7 | PRD311 | 2.2 |
| 25 | PD11 | 4.4 | PD13 | 2.5 | PD31 | 3.0 |
| | PR11 | 5.3 | PR13 | 4.6 | PR31 | 4.2 |
| | PRD111 | 1.9 | PRD133 | 1.1 | PRD311 | 2.8 |
| 30 | PD11 | 6.4 | PD13 | 3.8 | PD31 | 4.1 |
| | PR11 | 7.4 | PR13 | 6.9 | PR31 | 5.4 |
| | PRD111 | 5.0 | PRD133 | 2.1 | PRD311 | 4.8 |
| 40 | PD11 | 9.5 | PD13 | 6.1 | PD31 | 6.3 |
| | PR11 | 20.7 | PR13 | 18.1 | PR31 | 13.0 |
| | PRD111 | 6.4 | PRD133 | 2.5 | PRD311 | 8.9 |

**Table 3**
Conductivity data of POMA–RNA, POMA–DNA, POMA–RNA–DNA hybrids of different compositions at 30 °C.

| Composition | $\sigma$ (S/cm) | Composition | $\sigma$ (S/cm) | Composition | $\sigma$ (S/cm) |
|---|---|---|---|---|---|
| PR10 | $3.2\times10^{-5}$ | PD10 | $3.2\times10^{-5}$ | – | – |
| PR01 | $3.9\times10^{-9}$ | PD01 | $1.3\times10^{-10}$ | – | – |
| PR31 | $6.0\times10^{-6}$ | PD31 | $8.9\times10^{-6}$ | PRD311 | $1.1\times10^{-7}$ |
| PR11 | $1.0\times10^{-6}$ | PD11 | $5.3\times10^{-6}$ | PRD111 | $7.2\times10^{-8}$ |
| PR13 | $3.0\times10^{-6}$ | PD13 | $0.98\times10^{-6}$ | PRD133 | $2.2\times10^{-8}$ |

PR hybrid starts earlier than that in the PD system at all temperatures (Suppl. Fig. 5). Probably, the physical force for adsorption of POMA is stronger in the PR system than that in the PD system, decreasing the restoring effect of thermal fluctuation on the chain conformation. This is supported from the FTIR spectra where three types of interactions (viz. ionic, H-bonding and $\pi$–$\pi$) prevail compared to the only ionic interaction in the PD system [18]. This interesting UV results may be useful for RNA or DNA/RNA hybrid diagnostics.

Here it is interesting to compare the pH vs. time plot with $\lambda_{max}$ vs. log time plot for the hybrids at 30 °C (Suppl. Fig. 6). It indicates that the time of leveling is the same (i.e. 30 h) for both the processes and hence complexation and uncoiling of POMA is occurring in a concerted fashion. As POMA gets uncoiled, some –NH– groups become free and they complex immediately with $RNA^-$. To confirm that the red shift is occurring due to the conformational transition, Arrhenius plots (Fig. 8 and Suppl. Fig. 7) are made by taking $1/t_{780}$ as the rate constant of the process ($t_{780}$ is the time (h) to reach intermediate of the sudden hike, i.e. $\lambda_{max}$ value of 780 nm). In all cases the data fit in a good straight line. The activation energy values obtained from the least square slope are presented in Table 1 and they are in the range of 13–15 kcal/mol which is the same as in the PD system [17,18]. This value is also close to the activation energy values for conformational transition of poly(vinylidene fluoride) and poly(3-hexyl thiophene) [40,41] supporting that the conformational transition is the cause for the red shift in the UV–vis spectra.

*3.5.2. Shift of polaron band in POMA–RNA–DNA (PRD) system*

It is interesting to study the UV–vis spectra of PRD hybrid solution (Fig. 9(a)), as during transcription of genes, RNA forms stable complex with DNA [19,20]. The $\pi$–$\pi^*$ transition peaks and the polaron band to $\pi^*$ transition bands are almost the same as in the PR system but there is some difference in the shift of $\pi$-band to polaron band transition peak with time. In Fig. 9(b) a representative plot of $\lambda_{max}$ against log time is shown for PR11, PD11 and PR111 for 25 °C indicating that the uncoiling of POMA is much faster on the RNA surface than that on the dsDNA. This is true for all the temperatures studied (e.g. 20, 25, 30, and 40 °C; Table 2).

From the table it is also evident that in the PRD hybrid solutions the uncoiling of POMA is slower than that of PR and PD hybrids. To understand the reason of slowness in the PRD systems activation energy values are calculated from the Arrhenius plots (Suppl. Fig. 8) and the values are also presented in Table 1. It is apparent that the activation energy values of uncoiling in the PRD triplexes are almost the same with that in the PR or PD duplexes. So, the uncoiling rate of POMA in the PRD triplex is comparable to that in the PR and PD duplexes. The slowness of doping may therefore be considered due to the disorder arrangement of phosphate groups in the RD hybrids where POMA (ES) requires some extra time to search for the phosphate anions required for electrostatic interaction. Once POMA chains get adsorbed on the RD hybrid surface, the co-operative uncoiling of POMA chain starts at the same rate as in the PR and PD hybrids yielding the same activation energy. So we can conclude that the attachment of POMA chains is slower in the PRD hybrids than that in the PD or PR hybrids because of the more disordered array of the phosphate groups in the PRD hybrids. The larger the concentration of RD in the PRD hybrids, the longer the delay is due to the larger disorderliness in the array of the phosphate groups. So it may be concluded that the initiation of complexation is easier in the PR/PD system compared to that in the PRD system. The progress of complexation and uncoiling occurs in a concerted fashion and the uncoiling rate is almost the same in all the systems signifying the same cause (viz. repulsive interaction of radical cations) for the uncoiling process.

*3.6. Conductivity*

The dc conductivity values of POMA (ES), NaDNA, RNA, PD, PR and PRD samples are compared at 30 °C in Table 3. It is apparent from the table that pure RNA has a conductivity of $4.0\times10^{-9}$ S/cm which is approximately one order higher than that of pure DNA. The conductivity values of pure DNA and RNA is reported in literature

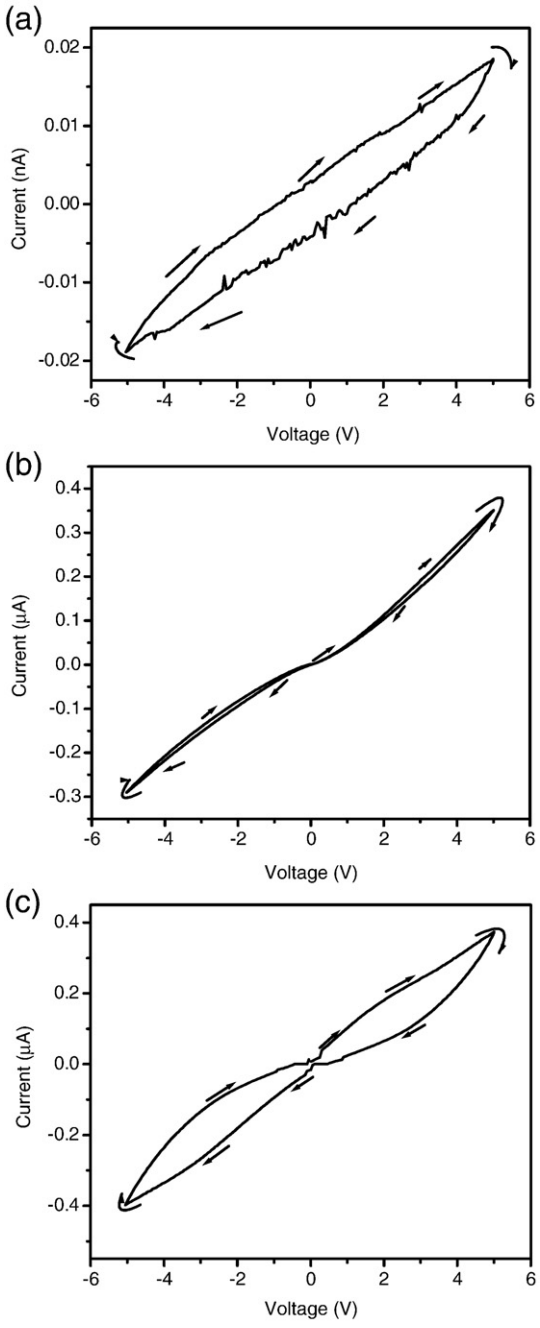


**Fig. 10.** Current–Voltage (*I*–*V*) characteristic curves of (a) RNA, (b) PR11 and (c) PRD111 hybrids.

($2\times10^{-12}$ S/cm) [42]. The two order higher values of conductivity in the present samples than that of the reported values might be due to the different nature of the samples produced from the different sources [17,43,44]. In the PR hybrids the conductivity values have increased by 3 orders than that of pure RNA and with increasing the less conducting RNA and DNA concentrations in the hybrids, the conductivity of hybrids gradually decreases. However, the same order of conductivity in the PR and PD hybrids of different compositions indicates that the charge carriers are only the POMA chains, the biological molecules (DNA/RNA) do not take part in the transport property of the hybrid. In the PRD triplexes the dc conductivity values are ~2 orders lower than that of the PD or PR duplexes, indicating more disordered structure of POMA in the triplexes than that in the duplexes. Probably, the POMA chain traverses both DNA and RNA helixes during wrapping introducing more disorder in the chain. Also the decrease of weight percent of POMA in the PRD systems compared to that of PR/PD systems is another cause of lowering of conductivity. To check if there is any contribution of ions e.g. $Na^+$, $NH_4^+$ and $Cl^-$ on the conductivity of the hybrids we have dialyzed the PR11, PD11 and PRD111 hybrids to remove the ions and the conductivity values of the dialyzed samples are $0.97\times10^{-6}$, $3.9\times10^{-6}$ and $6.66\times10^{-8}$ S/cm, respectively. The data are almost equal to those presented in Table 3 indicating that the conductivity is electronic in nature and is mainly contributed from the doped POMA chains in the hybrid.

### 3.7. I–V curves

In Fig. 10, the *I–V* characteristic curves of RNA, PR11 and PRD111 hybrids are presented. It is apparent from the figure that the RNA and the hybrids exhibit a hysterisis loop (for PR/PD hybrids as the scale is $10^3$ times higher, the gap is low (Suppl. Fig. 9)), i.e. in the forward bias at an applied voltage current is higher but in the backward bias at the same voltage the current is lower. Possibly there is a charge separation in the system that adds to the current in the forward bias but in the reverse bias the current is low due to the opposition by the separated charges. In the PR complex $RNA^-$ strongly binds the cationic charge of POMA (ES) through electrostatic interaction causing a lesser charge separation (cf. pH study). Again in the PRD111 hybrid hysterisis loop is larger, indicating an existence of a large charge separation that adds to the current for the forward bias but reduces in the reverse bias. This result also supports that in the PRD triplex the POMA is not so firmly attached as in the PR sample. So it may be concluded from the *I–V* curves that both PR and PRD hybrids are good semiconductors which may be used in biosensing appliances.

## 4. Conclusion

Biomolecular hybrids of a conducting polymer (POMA) and RNA are prepared at three different compositions and the TEM micrographs indicate a fibrillar network structure in all the hybrids. The FTIR spectra indicate an electrostatic interaction of phosphate anions of RNA with radical cations of POMA. Also there are H-bonding and $\pi$–$\pi^*$ interaction in the complexes and the interactions cause an intimate mixing of the components decreasing the in-plane vibration of bases of RNA. The CD spectra indicate a small distortion of A-RNA conformation towards its B form during the hybrid formation. The UV–vis spectra show a slow change of $\pi$-band to polaron band transition peak indicating the uncoiling of POMA chain on the RNA surface. It takes about 30 h to complete the uncoiling process but it takes about 100 h in the PRD complexes. The repulsive interaction of radical cations of POMA on the RNA surface is the cause of conformational change leading to a slow increase in conjugation length causing the slow red shift. A comparison of $\lambda_{max}$ vs. log time plot of PRD111 and PR11 indicates that the uncoiling in PRD111 starts at a longer time than that of PR11, possibly due to the disorder arrangement of the phosphate groups in the DNA–RNA hybrids. However, the activation energy is the same in both the PR and PRD hybrids, indicating that the uncoiling rate in triplexes is the same as that in duplexes. The delayed onset of uncoiling is due to the difficulty in complexation in the mixed RD hybrids. The conductivity values of PR hybrids are in the order of $10^{-6}$ S/cm whose value is three order higher than that of RNA, indicating that the PR hybrid would be useful for fabricating good biosensors. However, in the PRD hybrids the conductivity is decreased by two orders due to the disordered arrangement of POMA chains compared to that in the PR/PD duplexes. The *I–V* characteristic curves of PR and PRD hybrids are semiconducting in nature. The large hysterisis loop in PRD triplex compared to that of PR duplex in the *I–V* curves indicates that the POMA chain is more disordered in the triplex than that in the PD/PR duplexes. The spectral and conductivity data indicate possible use of the hybrid in RNA or RNA/DNA hybrid diagnostics and in making biosensors.

## Acknowledgment

P. Routh and P. Mukherjee acknowledge CSIR, New Delhi for granting fellowships.

## Appendix A. Supplementary data

Supplementary data associated with this article can be found, in the online version, at doi:10.1016/j.bpc.2009.05.004.

## References

[1] G.G. Wallace, L.A.P. Kane-Maguire, Manipulating and monitoring biomolecular interactions with conducting electroactive polymers, Adv. Mater. 14 (2002) 953–960.
[2] K.P.R. Nilsson, A. Herland, P. Hammarstrom, O. Inganas, Conjugated polyelectrolytes: conformation-sensitive optical probes for detection of amyloid fibril formation, Biochemistry 44 (2005) 3718–3724.
[3] K.P.R. Nilsson, O. Inganas, Chip and solution detection of DNA hybridization using a luminescent zwitterionic polythiophene derivative, Nature Materials 2 (2003) 419–424.
[4] B.S. Gaylord, A.J. Heeger, G.C. Bazan, DNA hybridization detection with water-soluble conjugated polymers and chromophore-labeled single-stranded DNA, J. Am. Chem. Soc. 125 (2003) 896–900.
[5] L.A. Thompson, J. Kowalik, M. Josowicz, J. Janata, Label-free DNA hybridization probe based on a conducting polymer, J. Am. Chem. Soc. 125 (2003) 324–325.
[6] J. Wang, M. Jiang, Toward genolelectronics: nucleic acid doped conducting polymers, Langmuir 16 (2000) 2269–2274.
[7] H.-A. Ho, A. Najari, M. Leclerc, Optical detection of DNA and proteins with cationic polythiophenes, Acc. Chem. Res. 41 (2008) 168–178.
[8] J.M. Gibbs, S.-J. Park, D.R. Anderson, K.J. Watson, C.A. Mirkin, S.T. Nguyen, Polymer-DNA hybrids as electrochemical probes for the detection of DNA, J. Am. Chem. Soc. 127 (2005) 1170–1178.
[9] N. Lassalle, P. Mailley, E. Vieil, T. Livache, A. Roget, J.P. Correia, L.M. Abrantes, Electronically conductive polymer grafted with oligonucleotides as electrosensors of DNA: preliminary study of real time monitoring by in situ techniques, J. Electroanal. Chem. 509 (2001) 48–57.
[10] B. Liu, G.C. Bazan, Interpolyelectrolyte complexes of conjugated copolymers and DNA: platforms for multicolor biosensors, J. Am. Chem. Soc. 126 (2004) 1942–1943.
[11] E.J. Finnegan, M.A. Matzke, The small RNA world, J. Cell Sci. 116 (2003) 4689–4693.
[12] M.W. Hentze, E. Izaurralde, B. Séraphin, A new era for the RNA world conference: RNA 2000, EMBO reports 5 (2000) 394–398.
[13] C.L. Recksiedler, B.A. Deore, M.S.A. Freund, Novel layer-by-layer approach for the fabrication of conducting polymer/RNA multilayer films for controlled release, Langmuir 22 (2006) 2811–2815.
[14] Y. Fan, X. Chen, A.D. Trigg, C.-h. Tung, J. Kong, Z. Gao, Detection of microRNAs using target-guided formation of conducting polymer nanowires in nanogaps, J. Am. Chem. Soc. 129 (2007) 5437–5443.
[15] O. Medalia, M. Heim, R. Guckenberger, R. Sperling, J. Sperling, Gold-tagged RNA — a probe for macromolecular assemblies, J. Struct. Biol. 127 (1999) 113–119.
[16] D. Liu, L.A. Gugliotti, T. Wu, M. Dolska, A.G. Tkachenko, M.K. Shipton, B.E. Eaton, D.L. Feldheim, RNA-mediated synthesis of palladium nanoparticles on Au surfaces, Langmuir 22 (2006) 5862–5866.
[17] (a) A. Dawn, A.K. Nandi, Biomolecular hybrid of a conducting polymer with DNA: morphology, structure, and doping behavior, Macromol. Biosci. 5 (2005) 441–450; (b) A. Dawn, A.K. Nandi, Slow doping rate in DNA–poly(*o*-methoxyaniline) hybrid: uncoiling of poly(*o*-methoxyaniline) chain on DNA template, Macromolecules 38 (2005) 10067–10073.
[18] (a) A. Dawn, A.K. Nandi, Simple method for the preparation of DNA–poly(*o*-methoxyaniline) hybrid: structure, morphology, and uncoiling of poly(*o*-methoxyaniline) on the DNA surface, Langmuir 22 (2006) 3273–3279;

(b) A. Dawn, A.K. Nandi, Nanostructured self-assembly of double-stranded DNA/poly(*o*-methoxyaniline) hybrid, J. Phys. Chem. C 111 (2007) 6268–6274.
[19] D.A. Erie, The many conformational states of RNA polymerase elongation complexes and their roles in the regulation of transcription, Biochim. Biophys. Acta 1577 (2002) 224–239.
[20] A. Shilatifard, R.C. Conaway, J.W. Conaway, The RNA polymerase II elongation complex, Ann. Rev. Biochem. 72 (2003) 693–715.
[21] L.H.C. Mattoso, R.M. Faria, L.O.S. Bulhões, A.G. MacDiarmid, Synthesis, doping, and processing of high molecular weight poly(*o*-methoxyaniline), J. Polym. Sci.: Part A: Polym. Chem. 32 (1994) 2147–2153.
[22] A. Andreatta, Y. Cao, J.C. Chiang, A.J. Heeger, P. Smith, Electrically-conductive fibers of polyaniline spun from solutions in concentrated sulfuric acid, Synthetic Metals 26 (1988) 383–389.
[23] D.G. Baird, J.K. Smith, Dilute solution properties of poly(1,4-phenylene terephthalamide) in sulfuric acid, J. Polym. Sci. Polym. Chem. 16 (1978) 61–70.
[24] A. Dawn, A.K. Nandi, Formation of silver nanoparticles in deoxyribonucleic acid–poly(*o*-methoxyaniline) hybrid: a novel nano-biocomposite, J. Phys. Chem. B 110 (2006) 18291–18298.
[25] (a) Armin U. Metzger, Thomas Schindler, Dieter Willbold, Margot Kraft, Clemens Steegborn, Andrea Volkmann, Rainer W. Frank, Paul Rosch, Structural rearrangements on HIV-1 Tat (32–72) TAR complex formation, FEBS Lett. 384 (1996) 255–259;
(b) H. Arakawa, J.F. Neault, H.A. Tajmir-Riahi, Silver(I) complexes with DNA and RNA studied by Fourier transform infrared spectroscopy and capillary electrophoresis, Biophys. J. 81 (2001) 1580–1587.
[26] Tan Ruoying, Frankel D. Alan, Circular dichroism studies suggest that TAR RNA changes conformation upon specific binding of arginine or guanidine, Biochemistry 31 (1992) 10288–10294.
[27] T.G. Spiro, Biological Application of Raman Spectroscopy, John Wiley and Sons, 1987.
[28] D.M. Loprete, K.A. Hartman, Conditions for the stability of the B, C, and Z structural forms of poly(dG–dC) in the presence of lithium, potassium, magnesium, calcium, and zinc cations, Biochemistry 32 (1993) 4077–4082.
[29] E.B. Starikov, M.A. Semenov, V.Ya. Maleev, A.I. Gasan, Evidential study of correlated events in biochemistry: physicochemical mechanisms of nucleic acid hydration as revealed by factor analysis, Biopolymers 31 (1991) 255–273.
[30] L.E. Prevette, T.E. Kodger, T.M. Reineke, M.L. Lynch, Deciphering the role of hydrogen bonding in enhancing pDNA–polycation interactions, Langmuir 23 (2007) 9773–9784.
[31] H. Arakawa, R. Ahmad, M. Naoui, H.-A. Tajmir-Riahi, A comparative study of calf thymus DNA binding to Cr(III) and Cr(VI) ions. Evidence for the guanine N-7-chromium-phosphate chelate formation, J. Biol. Chem. 275 (2000) 10150–10153.
[32] E. Taillandier, J. Liquier, J.A. Taboury, Advances in Infrared and Raman Spectroscopy, 1985.
[33] S. Brahms, J. Brahms, J. Pilet, Infrared studies on the backbone conformation of nucleic acids, Isr. J. Chem. 12 (1974) 153–163.
[34] H.A. Tajmir-Riahi, J.F. Neault, M. Naoui, Does DNA acid fixation produce left-handed Z structure? FEBS Lett. 370 (1995) 105–108.
[35] H.A. Tajmir-Riahi, M. Langlais, R. Savoir, A laser Raman spectroscopic study of the interaction of calf-thymus DNA with Cu(II) and Pb(II) ions: metal ion binding and DNA conformational changes, Nucleic Acids Res. 16 (1988) 751–762.
[36] (a) W.S. Huang, A.G. MacDiarmid, Optical properties of polyaniline, Polymer 34 (1993) 1833–1845;
(b) Y. Xia, J.M. Wiesinger, A.G. MacDiarmid, A.J. Epstein, Camphorsulfonic acid fully doped polyaniline emeraldine salt: conformations in different solvents studied by an ultraviolet/visible/near-infrared spectroscopic method, Chem. Mater. 7 (1995) 443–445.
[37] J. Stejskal, P. Kratochvíl, N. Radhakrishnan, Polyaniline dispersions 2. UV–Vis absorption spectra, Synthetic Metals 61 (1993) 225–231.
[38] J. Ruokolainen, H. Eerikainen, M. Torkkeli, R. Serimaa, M. Jussila, O. Ikkala, Comb-shaped supramolecules of emeraldine base form of polyaniline due to coordination with zinc dodecyl benzenesulfonate and their plasticized self-organized structures, Macromolecules 33 (2000) 9272–9276.
[39] A. Garai, B.K. Kuila, A.K. Nandi, Montmorillonite clay nanocomposites of sulfonic acid doped thermoreversible polyaniline gel: physical and mechanical properties, Macromolecules 39 (2006) 5410–5418.
[40] (a) P.V. Shibaev, K. Schaumburg, T. Bjornholm, K. Norgaard, Conformation of polythiophene derivatives in solution, Synthetic Metals 97 (1998) 97–104;
(b) S. Malik, T. Jana, A.K. Nandi, Thermoreversible gelation of regioregular poly(3-hexylthiophene) in xylene, Macromolecules 34 (2001) 275–282.
[41] (a) B.L. Farmer, A.J. Hopfinger, J.B. Lando, Polymorphism of poly(vinylidene fluoride): potential energy calculations of the effects of head-to-head units on the chain conformation and packing of poly(vinylidene fluoride), J. Appl. Phys. 43 (1972) 4293–4303;
(b) S. Mal, A.K. Nandi, Gelation mechanism of thermoreversible poly(vinylidene fluoride) gels in glyceryl tributyrate, Polymer 39 (1998) 6301–6307;
(c) A.K. Dikshit, A.K. Nandi, Thermoreversible gelation of poly(vinylidene flouride) in diethyl adipate: a concerted mechanism, Macromolecules 31 (1998) 8886–8892.
[42] D.D. Eley, D.I. Spivey, Semiconductivity of organic substances, part 9 — nucleic acid in the dry state, Trans. Faraday Soc. 58 (1962) 411–415.
[43] D. Porath, A. Bezryadin, S.D. Vries, C. Dekker, Direct measurement of electrical transport through DNA molecules, Nature 403 (2000) 635–638.
[44] Y.A. Berlin, A.L. Burin, M.A. Ratner, Charge hopping in DNA, J. Am. Chem. Soc. 123 (2001) 260–268.